



Local diffusion indicators: A new tool for analysis of electrochemical mass transport

Joseph R. Elliott, Richard G. Compton^{*}

Department of Chemistry, Physical and Theoretical Chemistry Laboratory, University of Oxford, South Parks Road, Oxford OX1 3QZ, Great Britain

ARTICLE INFO

Keywords:

Diffusion indicator
Mass transport
Diffusion
Chronoamperometry
Sphere on a plane
Micro-disc electrode

ABSTRACT

The recently introduced diffusion indicator (Haonan et al, J. Electroanal. Chem., 2019, 855, 113602) is generalised to characterise local mass transport fluxes to a non-uniformly accessible electrode to probe both qualitatively and quantitatively the nature of the diffusion to different parts of an electrode surface at different times following electrochemical perturbation. The approach is illustrated in respect of diffusion to a truncated sphere on a plane surface. The relative contributions of thin layer, linear and convergent diffusion following potential step chronoamperometry are evaluated. Comparison is made with analogous measurements on a micro-disc electrode. The results have implications for the transients accompanying the impact of nanoparticles on planar electrodes and for hanging mercury drop electrodes.

1. Introduction

Recent developments with nanoparticle-modified electrodes [1–5], single-entity electrochemistry [6–8] and nano-impact electrochemistry [9–13], as well as the continued prevalence of more traditional techniques such as those involving the hanging mercury drop electrode [14], emphasise the importance of developing a complete understanding of diffusional transport towards electrochemically active spheres in contact with supporting, planar surfaces.

Numerical simulation [15–17] and multipole methods [18] have been used to derive results for such systems under both steady-state conditions and during voltammetry. The limiting steady-state current for a full sphere on a surface is well-established [15–18] and requires a correction factor of $\ln(2)$ relative to the corresponding expression for an isolated sphere:

$$I_{lim} = 4\pi \ln(2)FDc^*r_e \quad (1)$$

Additional correction factors have been proposed for the steady-state current to spheres of differing contact angles via a ‘shape factor’ by Bobbert [18]. Theory and experiment have been combined to describe the behaviour of randomly-distributed arrays of spherical nanoparticles on a surface, namely the transitions between 4 diffusional regime cases [16]. However, insufficient consideration has been given to more physically realistic cases where the physical contact

between the particle and surface is not infinitesimally small. Such cases can be effectively modelled with spheres truncated by the surface with contact angles, θ_c , below 180° or π (see Fig. 1).

In this work we present numerical simulations of chronoamperometry at a variably truncated sphere on a supporting plane. A simple mapping of results from an isolated sphere is presented to approximate the flux transient for a sphere on a surface. This mapping demonstrates an error of $< 1.5\%$ throughout the current transient and may also be applied to truncated spheres, with similar accuracy for $\theta_c \geq \pi/4$.

The diffusion indicator, α , has been recently established by Le et al [19] as a means to quantitatively characterise the extent to which diffusion to the electrode is convergent ($\alpha = 1$) or linear/Cottrellian ($\alpha = 0$), and is defined by:

$$\alpha = 2 \frac{d(\log(J))}{d(\log(T))} + 1 \quad (2)$$

where J and T are surface flux and time, respectively, in either dimensional or dimensionless forms. Several subsequent investigations into diffusion-limited interfacial processes occurring on various geometries have made use of this indicator [20–23]. This diffusion indicator is here used to analyse the transition from linear to convergent diffusion [24,25] for the sphere on a surface and to compare with the transitions observed for isolated spheres and disks.

Novelly, the diffusion indicator is applied to the local flux J_{local} to give α_{local} , rather than as hitherto to the total flux, allowing observation of changes to the diffusion regime local to specific points on the sup-

^{*} Corresponding author.

E-mail address: richard.compton@chem.ox.ac.uk (R.G. Compton).

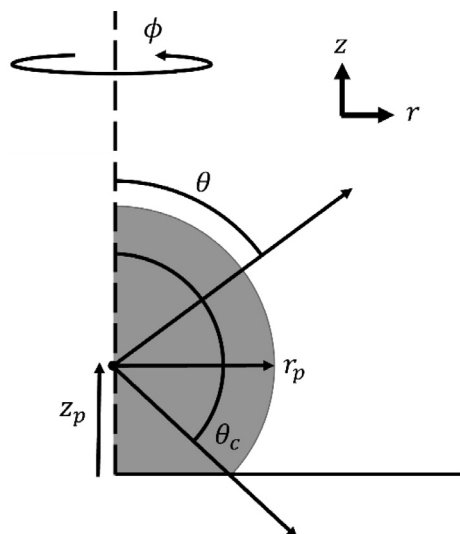


Fig. 1. Illustration of the simulation space used for a truncated spherical grey particle on a surface. The cylindrical polar coordinate system (r, z, ϕ) is presented along with the axis of symmetry (dashed). Other key spatial parameters are also illustrated: the polar angle θ , the polar contact angle θ_c , the particle radius r_p , and the perpendicular distance from the plane to the particle centre z_p .

ported sphere. These results evidence the temporal development of a stagnation zone between the sphere and plane and demonstrate an α_{local} minimum associated with the growth of this zone. This result is comparable with the results observed for thin-layer systems [22]. Results are presented for the full sphere on a surface, variably truncated spheres, and for a disk. α_{local} is thus presented as a means for investigating how diffusion-limited currents are affected by complex electrode geometries.

2. Methods

2.1. Coordinate system

The electrode system of interest involves a single, conductive, truncated, spherical particle of radius r_p in contact with a supporting infinite planar surface. This system is described using cylindrical polar coordinates (r, z, ϕ) with the origin at the centre of the contact area between the sphere and surface, where r is the perpendicular distance from the axis of symmetry, z is the coordinate normal to the planar surface, and ϕ is the angle about the axis of symmetry relative to an arbitrary reference direction normal to the axis. Symmetrical considerations demonstrate that no concentration gradients can develop along the ϕ coordinate; we thus simplify the system to a 2-dimensional simulation using (r, z) coordinates considering a single half-plane.

The polar angle θ , measured from the axis of symmetry away from the inert plane, is also used in this work to describe the position of a point on the particle surface; this is related to θ_c which describes the polar angle to the point of contact between the particle and cuticle, as illustrated in Fig. 1, which is equivalent to the particle's contact angle. The perpendicular distance between the plane and particle centre describes the extent of truncation and is represented by z_p .

2.2. Mass transport equations and boundary conditions

We consider a simple one-electron transfer:



Both species A and B are soluble and are assumed to possess equal diffusion coefficients. Only A is initially present in solution. We simulate the current transient produced by a potential jump to a large overpotential corresponding to diffusion-controlled reduction of A: therefore,

$$\text{at } t = 0 : c_A = c_A^*; c_B = 0 \forall (r, z) \quad (4)$$

$$t > 0 : c_A = 0; c_B = c_A^* (\text{for } r^2 + z^2 = 1) \quad (5)$$

where c_i denotes the concentration of species i and c_i^* denotes the bulk concentration of species i .

The mass transport of A and B in solution is described by Fick's second law of diffusion according to Eq. (6) for species i :

$$\frac{\partial c_i}{\partial t} = D_i \cdot \nabla^2 c_i = D_i \left\{ \frac{\partial^2 c_i}{\partial r^2} + \frac{1}{r} \frac{\partial c_i}{\partial r} + \frac{\partial^2 c_i}{\partial z^2} \right\} \quad (6)$$

where D_i denotes the diffusion coefficient of species i . Since mass must be conserved within the system and the diffusion coefficients for A and B are set to be identical, $c_A + c_B = c_A^*$ at all points in the system. As a result, only species A need be simulated in order to produce the current transient.

Zero-flux boundary conditions are applied normal to the symmetry axis and the inert, supporting planar surface. The bulk solution condition is implemented at a distance of $6\sqrt{Dt}$ from the particle surface, which is much further than the expected root mean squared distance travelled by a diffusing particle due to Brownian motion [26,27]: $\langle x \rangle_{rms} = \sqrt{6Dt}$.

2.3. Conversion to dimensionless coordinates

The system is normalised according to the dimensionless conversions given in Table 1.

I is the total current to the particle electrode and relates the dimensionless J_{Tot} to an experimentally measurable value.

Fick's second law of diffusion in dimensionless form is:

$$\frac{\partial C}{\partial T} = \frac{\partial^2 C}{\partial R^2} + \frac{1}{R} \frac{\partial C}{\partial R} + \frac{\partial^2 C}{\partial Z^2} \quad (7)$$

2.4. Calculating the current

The dimensionless flux of species A to the particle is equal to the dimensionless concentration gradient normal to the particle surface through Fick's first law of diffusion. Using the cylindrical coordinate system, the dimensionless flux must be determined from its R - and Z - components:

$$J = \frac{\partial C}{\partial R} \sin(\theta) + \frac{\partial C}{\partial Z} \cos(\theta) \quad (8)$$

The total dimensionless flux is calculated by the integration of J across the electrode surface:

Table 1
Dimensionless conversions used for the simulation system.

Dimensionless Parameter	Expression
Radial coordinate	$R = r/r_p$
Normal coordinate	$Z = z/r_p$
Normal distance from plane to sphere centre	$Z_p = z_p/r_p$
Time	$T = D_A t / r_p^2$
Concentration of species A	$C = c_A / c_A^*$
Local electrode flux	$J = \frac{J_{r_p}}{D_A c_A^*}$
Total electrode flux	$J_{Tot} = \frac{I}{FD_A c_A^* r_p} = 2\pi \int_0^{\theta_c} J \cdot \sin(\theta) d\theta$

$$J_{Tot} = 2\pi \int_0^{\theta_c} J \cdot \sin(\theta) d\theta \quad (9)$$

2.5. Simulation procedure

The mass transport equation and associated boundary conditions are discretised according to the following scheme and as illustrated in Fig. 2.

The coordinate system chosen requires a high mesh density about the curved surface of the sphere to accurately describe the surface and diffusion proximal to it. This is ensured by arranging the grid such that each row within $0 < Z < 1 + Z_p$ contains a single point on the sphere surface satisfying $R = \sqrt{1 - (Z - Z_p)^2}$: thus the curved surface is described by consistent steps in the grid and the spatial mesh density about the sphere is described singly by the constant $d\theta$. Since less precision is required at a distance from the sphere, the grid expands as it moves beyond $R = 1$ and $Z = 1 + Z_p$. The grid expansion is achieved exponentially [28–31] such that:

- For $R > 1$: $R_i = R_{i-1} + h_R \cdot \omega_R^{i-1}$
- For $Z > 1 + Z_p$: $Z_i = Z_{i-1} + h_Z \cdot \omega_Z^{i-1}$

where h_R and h_Z are the smallest spacings possible in the R - and Z -directions respectively, and ω_R and ω_Z are expansion factors in the R - and Z - directions respectively.

A backward implicit discretization [32–34] is used to resolve the steps in time. An exponentially expanding time grid is used for the temporal discretisation.

This discretised, finite difference system is then solved fully implicitly and iteratively using the Biconjugate Gradient Stabilised method (BICGSTAB), with a relative convergence tolerance of 1×10^{-6} , with a semi-coarsening multigrid (SMG) preconditioner. The numerical simulation was performed on a Linux(Centos) machine with an Intel Core i7-6800 K CPU (3.40 GHz, 6 cores), 32 GB of RAM, and an Nvidia Quadro GP100. The simulation program was written in C++ , utilis-

ing the HYPRE software package (version 2.18.2) [35,36] executed with CUDA enabled GPU support. Construction of the discretised grid, data analysis, and plotting were performed with *python*, including the *NumPy*, *SciPy* and *matplotlib* packages.

The flux transient was divided into windows of time which were simulated simultaneously with individually tailored grid parameters and then concatenated to efficiently produce a full flux transient.

3. Results & discussion

In this section we consider different cases of the truncated spherical particle on a plane and simulate flux profiles resulting from an applied potential jump from zero current to one such that complete reduction of A occurs on the particle surface. We begin by considering the total flux for the cases of a hemisphere on a plane and a perfect sphere on a plane before considering spheres more generally, concluding with a comparison between greatly truncated spheres for which $\theta_c < \pi/2$ and the micro-disk electrode. We then consider local fluxes across the electrode surfaces and introduce the local diffusion indicator, α_{local} , and their variation across the electrode surface to understand the causes underpinning the observed diffusion-controlled response and identifying the role of local thin-layer like behaviour.

3.1. Total flux to a hemisphere and a sphere on a plane

The simplest possible case of a variably truncated sphere on a plane is the hemisphere, for which $\theta_c = \pi/2$. This case possesses polar angular isotropy; thus, the diffusion is simplified to one-dimension, the distance from the particle centre ρ . The dimensionless total flux transient to a hemispherical particle after a potential jump is soluble analytically [37] as

$$J_{Tot} = 2\pi \left(\frac{1}{\sqrt{\pi T}} + 1 \right) \quad (10)$$

The resulting flux transient is exactly one half that produced by a potential jump on a sphere isolated in solution. Due to its relative simplicity, this unidimensional system has been used to describe various problems involving a truncated sphere on a surface, such as the mercury drop electrode [38–40] and electrodes modified by mercury micro-droplets [41].

A second case is that of a perfect sphere with a point contact to a surface, and for which $\theta_c = \pi$. This has been considered previously both via theoretical analysis [18] and numerical simulation [15–17] and is used for the analysis of nanoparticle-modified electrode surfaces [1] and nano-impacts [12,42–44]. Fig. 3 illustrates the flux transient produced by numerical simulation for a full sphere on a surface compared to that of an isolated sphere. The full transition from linear diffusion to convergent diffusion is observed within the window $-4 \leq \log(T) \leq 3$. At short times the transients superimpose and the response is Cottrellian [45,46]. The dimensionless total flux thus evolves according to the equation:

$$J_{Tot} = \frac{4\sqrt{\pi}}{\sqrt{T}}, \quad (11)$$

reflecting linear diffusion across the full surface of the sphere. At longer times the response of the sphere on a surface drops below that of the isolated sphere as diffusional blocking by the surface becomes increasingly significant. In both cases at long times a steady-state current is established corresponding to convergent diffusion [24]. The steady-state current for the sphere on a plane has been shown [15,18] to be:

$$I_{lim} = 4\pi n(2)nFD_r p[A]_{bulk} \quad (12)$$

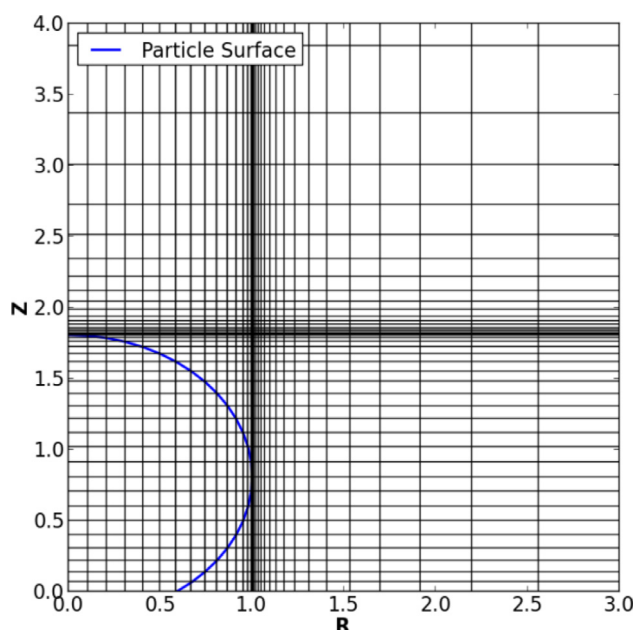


Fig. 2. Illustration of the spatial discretisation scheme used in this work proximal to the truncated sphere particle. The particle surface is represented by a blue line. Spatial coordinates are in dimensionless forms. The spatial parameters used are chosen purely for illustrative purposes and are as follows: $Z_p = 0.8$, $d\theta = \pi/30$ and $\omega_R = \omega_Z = 1.3$.

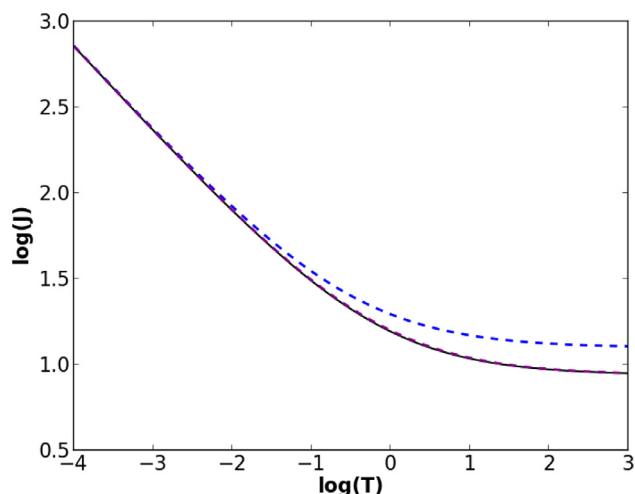


Fig. 3. Log-log plot of the simulated dimensionless total flux transient for a sphere on a surface (black solid) and results for the isolated sphere (blue dashed) and the empirical “modified sphere” (purple dashed) co-presented. It is observed that there is significant overlap between the simulated results and the empirical “modified sphere” equation which makes the curves difficult to distinguish graphically. The purple dashed curve of the “modified sphere” equation slightly overestimates the simulation results around $\log(T) = 0$.

It is useful to generate an analytical expression, analogous to Eq. (10), to approximate the full transient. On comparison of Eq. (12) with the steady-state current to an isolated sphere, the difference is the $\ln(2)$ factor. Thus we intuitively [17] modify the analytical result for the isolated sphere such that the theoretical short- and long-time limits of the sphere on a plane are accurately described. The resulting “modified sphere” equation, used to approximate the flux transient for a sphere on a plane, is:

$$J_{Tot} = 4\pi \left(\frac{1}{\sqrt{\pi T}} + \ln(2) \right) \quad (13)$$

This transient, approximating a sphere on a plane of radius r_p bathed in a solution of bulk concentration c^* , can be replicated by an isolated sphere with the radius $r_{isolated}$ in a solution of concentration $c_{isolated}^*$ if $r_{isolated} = 1.44 \times r_p$ and $c_{isolated}^* = 0.48 \times c^*$.

The approximation in Eq. (13) was compared with the fully converged simulation results for chronoamperometry on a sphere on a plane and found to be an excellent approximation, as shown in Fig. 3. Fig. 4 shows the relative error of the “modified sphere” equation from the simulated results for a sphere on a plane as given by

$$RelativeError = \frac{J_{Modified} - J_{Simulated}}{J_{Simulated}} \times 100\% \quad (14)$$

While the approximation is excellent in the short- and long-time limits (error < 0.3%), a maximum error of 1.48% is observed at $T = 0.67$. Since the converged simulation results are themselves accurate to within 0.1% of literature results [15–18] within the range $-4 \leq \log(T) \leq 3$, the total maximum error is 1.58%, which is likely to be more than adequate for most applications. The small error corresponds to an overestimation of the flux during the transition from linear to convergent diffusion.

It is insightful to apply the diffusion indicator, $\alpha = 2 \frac{d(\log(J))}{d(\log(T))} + 1$, to the flux transients shown in Fig. 3 and the resulting profiles produced for the sphere on a surface, the isolated sphere, and the “modified sphere” equation are presented in Fig. 5. Each profile shows a smooth transition between 0 and 1 corresponding to the transition from linear to convergent diffusion. It is seen that the sphere on a plane and “modified sphere” equation deviate in their diffusional behaviour from the isolated sphere only during the transition between the limiting

regimes. Although α has been previously demonstrated to act as a sensitive means to visualise changes in diffusional behaviour [19,20,22,23], only slight deviations from the “modified sphere” profile are noted. For developing a deeper understanding of the diffusional behaviour during this transitory period we introduce the idea of a local diffusion indicator, α_{local} , in the next section to provide further insights.

3.2. Local flux and local diffusion indicator profiles for a sphere on a plane ($\theta_c = \pi$)

A benefit of simulated systems is the ability to extract local flux transients from points on the electrode surface. For electrodes of complex geometry which exhibit non-uniform flux these local flux transients can possess valuable information on how the geometry affects the diffusion to the electrode. Just as the diffusion indicator, α , applied to the total flux transient provides information on the diffusional behaviour of the system about the electrode, a local diffusion indicator, applied to a local flux transient, can similarly quantify changes in the diffusional behaviour at a specific region of the system:

$$\alpha_{local} = 2 \frac{d(\log(J_{local}))}{d(\log(T))} + 1 \quad (15)$$

Fig. 6 and Fig. 7 present the local flux and local diffusion indicator, α_{local} , profiles for the sphere on a surface at regular θ -intervals about the surface. These are compared to the flux profiles and α profiles expected for an isolated sphere and the “modified sphere” equation. At short times, the local fluxes and α_{local} obey the profiles given by the isolated sphere as opposed to the “modified sphere” equation. However, the profiles for each θ negatively deviate from the isolated sphere at different points in time. A minimum in α_{local} develops for θ values above $\pi/2$, with a negative α_{local}^{min} observed for θ values close to π . The closer to θ_c , the earlier this deviation occurs and the more negative the α_{local}^{min} . At long time, all α_{local} values converge on to the “modified sphere” equation’s α profile irrespective of θ .

At short times, the diffusion layer is insufficiently thick for the inert surface to affect the surface flux and so the local fluxes initially obey the transient predicted for an isolated sphere. However, for $\theta > \pi/2$, at some point in time, the diffusion layer will reach the inert plane and the amount of material arriving to the surface solely along the vector normal to the sphere will begin to deplete.

This depletion of material between the sphere and plane is to some extent comparable to the depletion of a thin layer above a planar electrode, which has been investigated previously [22]. The analytically derived flux transient at a planar electrode under thin layer conditions [25] is:

$$J = 2 \sum_{m=1}^{\infty} \exp\left(-\frac{(2m-1)^2 \pi^2 T}{4}\right) \quad (16)$$

We present the resulting diffusion indicator for a depleting thin layer above a planar electrode:

$$\begin{aligned} \alpha &= 2T \frac{\sum_{m=1}^{\infty} \left(-\frac{(2m-1)^2 \pi^2}{4}\right) \exp\left(-\frac{(2m-1)^2 \pi^2 T}{4}\right)}{\sum_{m=1}^{\infty} \exp\left(-\frac{(2m-1)^2 \pi^2 T}{4}\right)} + 1 \\ &= 1 - \frac{\pi^2 T}{2} + \frac{\sum_{m=2}^{\infty} (-2m(m-1)\pi^2 T) \exp\left(-\frac{(2m-1)^2 \pi^2 T}{4}\right)}{\sum_{m=1}^{\infty} \exp\left(-\frac{(2m-1)^2 \pi^2 T}{4}\right)} \end{aligned} \quad (17)$$

The diffusion indicator in the long-time limit for a depleting thin-layer above a planar electrode can be approximated as: $\alpha \approx 1 - \frac{\pi^2}{2} T$ since the exponential terms decay to zero; thus, the diffusion indicator evidently tends towards negative infinity at long times in this system.

The zero-flux boundary at the plane in contact with the electroactive sphere also produces a depletion of material between it and

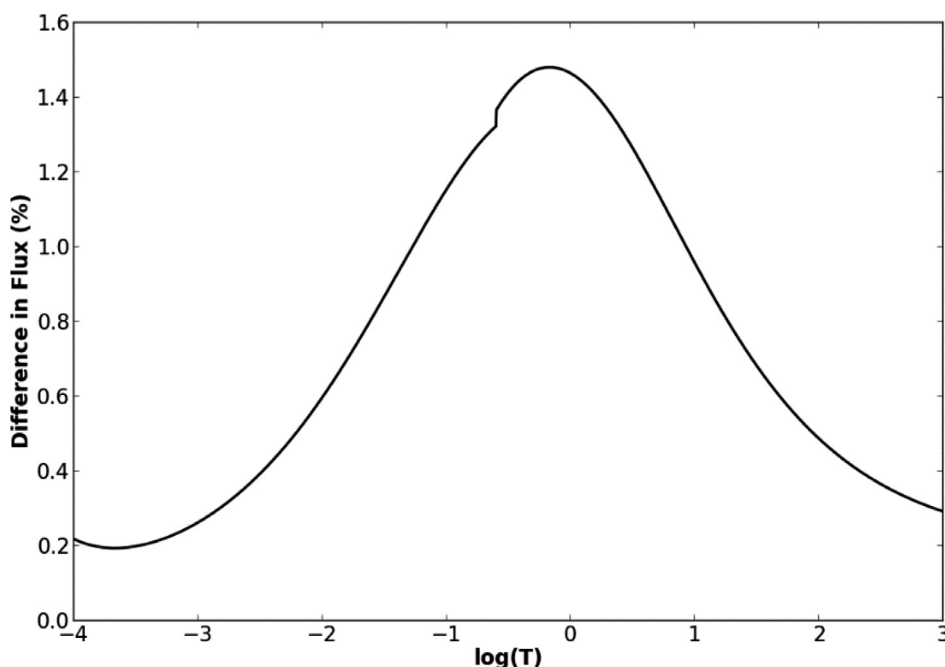


Fig. 4. Relative error of the total flux predicted by the “modified sphere” equation relative to the simulated results for a sphere on a surface expressed as a percentage of the simulated flux and as a function of logarithmic time. The discontinuity occurs at the point of transition between differently gridded zones of simulated time.

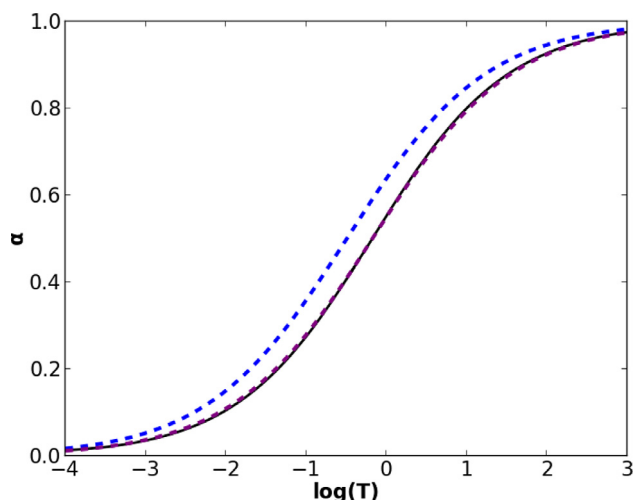


Fig. 5. Diffusion indicator (α) profile produced by simulation for a sphere on a surface (black solid) compared to the predictions for an isolated sphere (blue dashed) and the empirical “modified sphere” (purple dashed). It is observed that significant overlap between the purple dashed line and the solid black line makes them difficult to distinguish graphically. The purple dashed curve slightly overestimates the black curve before $\log(T) = 0$ and slightly underestimates it after $\log(T) = 0$ with good agreement at the short and long time limits.

the electrode. However, unlike the planar thin-layer system described by Eq. (16), additional material can arrive along the θ -coordinate for the sphere-on-a-plane system. This additional source of material counteracts the falling α_{local} , producing a finite minimum in α_{local} , and causes eventual convergence with the “modified sphere” equation’s α profile in the long-time limit.

A similar minimum, caused by the thin-layer-like depletion of material but replenished in part by arrival of material from an additional source, is also observed in the diffusion indicator profiles

demonstrated in recent work by Yang et al [47] in which layers of blocking spheres rest on a planar electrode. Material on the underside of the first layer of spheres is initially depleted until material above the sphere’s meridian acts as a new source of material. The diffusion indicator thus decreases to a finite minimum before increasing towards convergent diffusion as material on the sphere’s topside is forced to diffuse through a narrow pore between spheres. As the diffusion layer extends beyond the layer(s) of blocking spheres, α tends towards zero and Cottrellian behaviour again. Additional layers of spheres can produce a second peak in α . Features of these two peaks can then be analysed to determine geometrical features of the environment such as number of layers of spheres and the pore size between adjacent spheres.

Fig. 8 demonstrates the evolution with time of the $\frac{\partial C}{\partial \theta}$ gradient local to the electrode surface at various θ . It can be seen that, for $\theta < \pi/2$, the depletion of material at the planar surface (due to the lack of diffusion through it) results in the development of a relatively large, negative $\frac{\partial C}{\partial \theta}$ concentration gradient. $\frac{\partial C}{\partial \theta}$ goes through a minimum before tending towards a smaller steady state value. This corresponds to a reduction in the local flux normal to the surface and a negative gradient of the α_{local} profile, which generates a $\alpha_{\text{local}}^{\text{min}}$. The point at which α_{local} converges on to the “modified sphere” equation is the moment at which the $\frac{\partial C}{\partial \theta}$ gradient ceases to evolve with time at a given θ . Thus, α_{local} offers an elegant means of insight into the evolution of local concentration gradients parallel to the particle surface.

It is insightful to investigate the effect of the plane in contact with truncated spherical electrodes to correctly characterise the diffusional behaviour when the contact angle θ_c is neither π nor $\pi/2$. In order to effectively observe diffusional effects beyond the Cottrellian to convergent diffusion transition, the “modified sphere” equation (Eq. (13)) must be generalised for any θ_c .

3.3. Generalisation of the “modified sphere” equation for truncated spheres

The “modified sphere” equation (Eq. (13)) is used in this work as an approximation of the flux transient for a sphere on a plane and com-

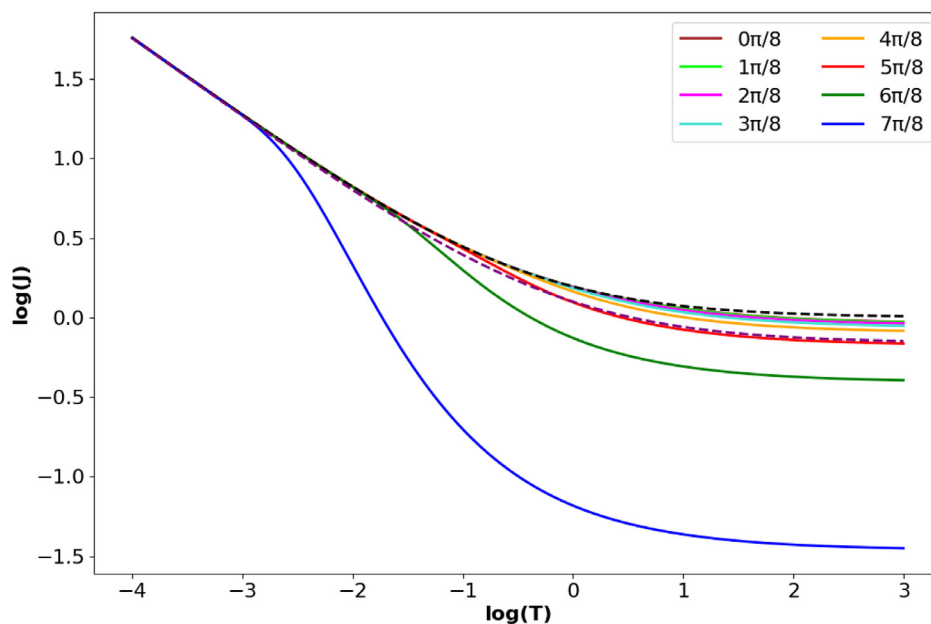


Fig. 6. Local flux transients for the sphere on a surface at different positions on the sphere surface. θ -values are used to describe the position on the surface and are given in the Figure legend. Flux transients for the isolated sphere (black dashed) and the “modified sphere” equation (purple dashed) are also presented.

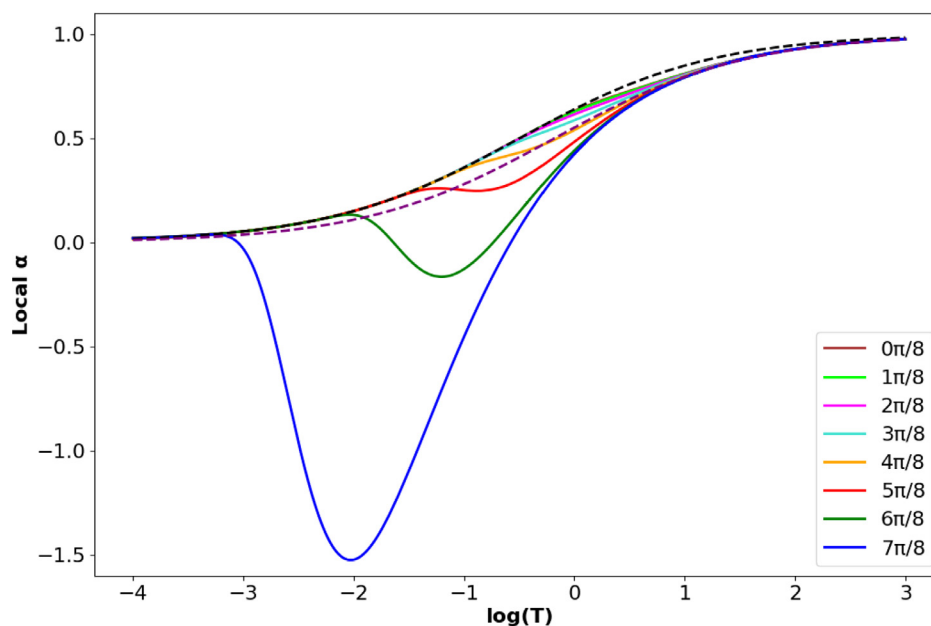


Fig. 7. Local diffusion indicator (α_{local}) profiles for the sphere on a surface at different positions on the sphere surface. θ -values are used to describe the position on the surface and are given in the Figure legend. Local diffusion indicator profiles for the isolated sphere (black dashed) and the “modified sphere” equation (purple dashed) are also presented.

parison to it is used as a means to assess how the diffusion to the sphere is affected by the presence of the inert plane. The “modified sphere” equation is derived by modifying results for an isolated sphere to approximate results for a sphere on a plane. Our use of this equation builds on work by Ward et al [17] in which steady-state voltammograms for a sphere on a plane were accurately generated by performing an inexpensive, one dimensional simulation of an isolated sphere followed by an appropriate mapping of the results using a conversion of c^* (bulk analyte concentration) and E_f (formal potential of the electron transfer). For chronoamperometry, we suggest the mapping of results through the conversion of c^* and r_p (the spherical particle radius).

The “modified sphere” equation is generally applicable for any truncated sphere in the form:

$$J = 2\pi \left(\frac{1 - \cos(\theta_c)}{\sqrt{\pi T}} + x \right) \quad (18)$$

where the $1 - \cos(\theta_c)$ factor corrects for the electrode surface area during the Cottrellian regime and $x = \int_0^{\theta_c} j_{ss} \sin(\theta) d\theta$ corresponds to the limiting dimensionless total steady-state flux for a given (r, z) slice. x may be calculated either using Bobbert’s table of shape factors [18] or from numerical simulation of $\frac{\partial c}{\partial t} = D \nabla^2 c = 0$.

Assuming a consistent value of the diffusion coefficient D , the flux transient produced by the “modified sphere” equation for a certain

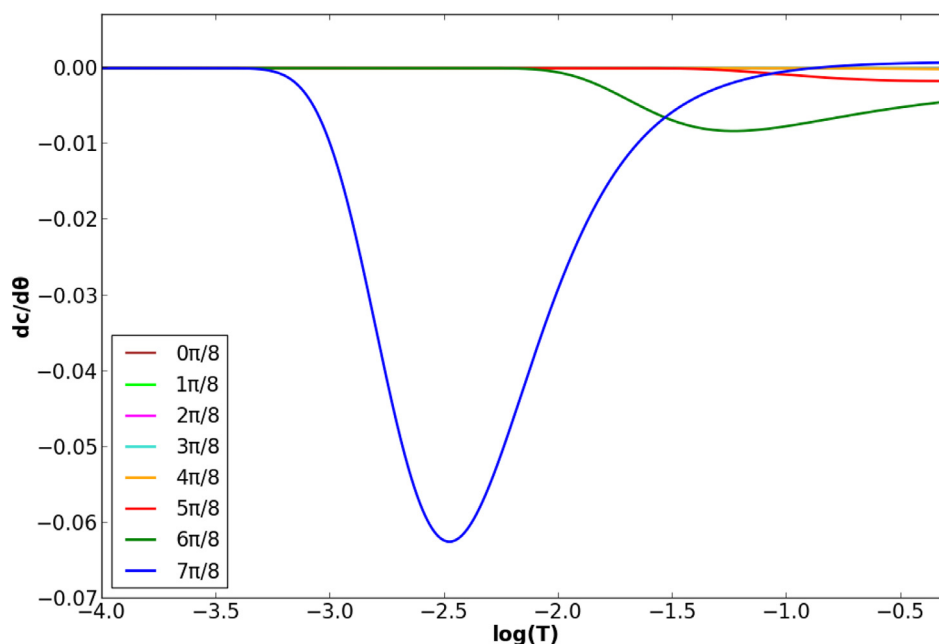


Fig. 8. Plots of local $\partial C/\partial \theta$ profiles on the surface of a sphere-on-a-plane electrode during chronoamperometry. These profiles are extracted from varying positions on the surface denoted by the θ -positions given in the Figure legend.

truncated sphere on a surface can be replicated by an isolated sphere under the following conditions:

$$r_{\text{isolated}} = r_{\text{truncated}} \frac{1 - \cos(\theta_c)}{x}$$

$$c_{\text{isolated}}^* = c_{\text{truncated}}^* \left(\frac{x^2}{1 - \cos(\theta_c)} \right)$$

We next apply the “modified sphere” equation to truncated spheres generally starting with the case of $\theta_c = 3\pi/4$.

3.4. Local diffusion indicator profiles for the $\theta_c = 3\pi/4$ truncated sphere on a plane

We seek insight into how the diffusional effects vary between the cases of a full sphere and a hemisphere on a plane. Numerical simulation of a potential jump on a spherical electrode truncated to produce a contact angle of $\theta_c = 3\pi/4$ was performed and total and local fluxes were extracted. Fig. 9 shows the local diffusion indicator profiles produced with comparison to the isolated sphere and the “modified sphere” equation (Eq. (18)). The values of θ were chosen to facilitate

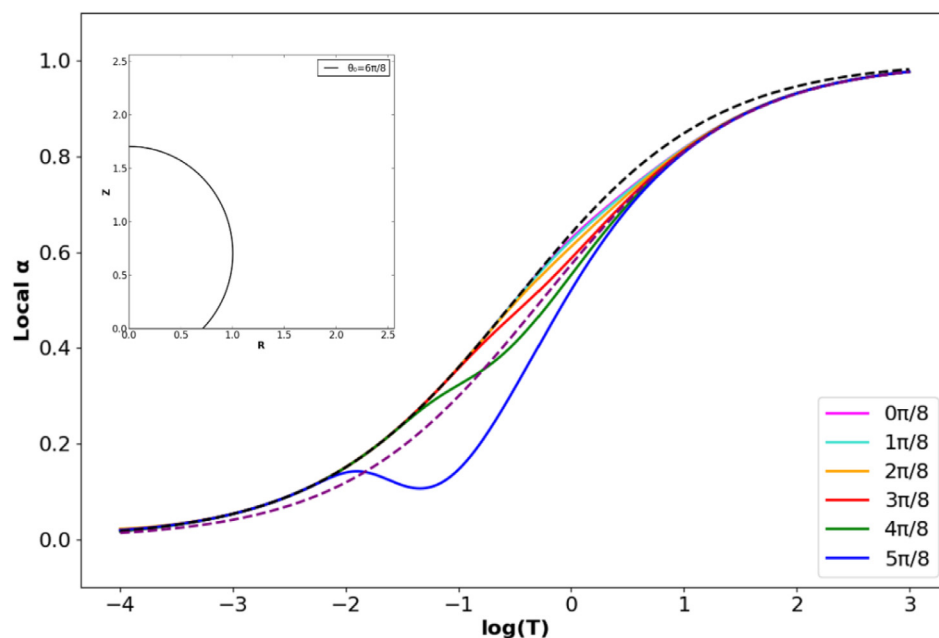


Fig. 9. Local diffusion indicator (α_{local}) profiles for the truncated sphere with contact angle of $\theta_c = 3\pi/4$. The θ -values at these positions are given in the Figure legend. The values for the isolated sphere (black dashed) and the “modified sphere” equation (purple dashed) are also presented. The inlaid diagram illustrates the shape of this truncated sphere electrode on the supporting plane.

comparison with the α_{local} profiles produced for the full sphere, demonstrated in Fig. 7.

Trends in the α_{local} profiles for $\theta_c = 3\pi/4$ are qualitatively similar to trends observed for the $\theta_c = \pi$ case. For the same θ , if $\theta > \pi/2$, an earlier and more pronounced minimum is observed, since that section of the sphere is now closer to the new contact point and also closer to the inert surface, giving a more pronounced local ‘thin-layer’ effect and an earlier development of local $\frac{\partial C}{\partial \theta}$. For $\theta < \pi/2$, the decreased θ_c results in a later and less pronounced deviation of α_{local} from the isolated sphere and a weaker overall $\frac{\partial C}{\partial \theta}$. This is a consequence of greater overall accessibility to the sphere-plane contact by diffusion and the greater similarity of the system to the hemisphere case.

3.5. Total and local diffusion indicator profiles for $\theta_c = \pi/4$, $\theta_c = \pi/8$, and comparison with a micro-disk electrode

Spheres truncated to a level beyond a hemisphere (i.e., $\theta_c < \pi/2$) are expected to display very different diffusional behaviour to what has been seen thus far. Rather than the contact point being concealed from the solution in a local thin-layer-like geometry, the contact point is instead more exposed to convergent diffusion from the bulk solution than the rest of the electrode surface. In the limit of small contact angle this geometry approaches that of the intensely studied [48–56] micro-disk, which possesses a fully exposed edge; the micro-disk is a limiting case for the truncated sphere [18] since the surface asymptotically approaches a flat surface as $\theta_c \rightarrow 0$.

In this section, we seek to investigate the transition between the limiting cases of near-sphere-like and near-disk-like diffusional behaviour as θ_c is decreased from a hemisphere towards $\theta_c = 0$. The former limit is characterised by the “modified sphere” equation (Eq. (18)) which considers only terms arising from linear and convergent diffusion such that no edge effect is seen. The latter limit is characterised by the Shoup-Szabo equation [48] (with a surface area correction according to θ_c), with significant edge diffusion which increases with time. While more recent approximations are available for characterising the limiting disk behaviour, such as those presented by Mahon and Oldham [54,55] and Bieniasz [56], the Shoup-Szabo equation is a simple and highly familiar result for electrochemists, whose maximum error of 0.6% satisfies experimental demands and the demands of this present work.

In the following, $\theta_c = \pi/4$ and $\theta_c = \pi/8$ are presented as informative cases. Profiles of α are presented in assessment of the utility of α for characterising the diffusional behaviour relative to the two limiting cases described above: namely the sphere behaviour with no edge effect and the disk behaviour with considerable edge effect.

Fig. 10 shows the α profiles for the cases of $\theta_c = \pi/4$ and $\theta_c = \pi/8$ in plots (A) and (B) respectively. The isolated sphere is presented as a blue dashed line, the “modified sphere” equation is presented as a purple dashed line, and the Shoup-Szabo equation is presented as a red dashed line. The α profile in (A) follows the “modified sphere” equation more closely than the Shoup-Szabo equation, while in (B) the α profile follows the latter equation more accurately. This illustrates a general transition between the two diffusional regimes: namely near-sphere-like to near-disk-like.

In Fig. 10(A), α follows the prediction of the “modified sphere” equation accurately at short times for $\theta_c = \pi/4$, however, after the “modified sphere” and Shoup-Szabo α profiles cross, α for the truncated sphere follows a curve located between these two limiting cases. Meanwhile in Fig. 10(B) for $\theta_c = \pi/8$, the Shoup-Szabo describes the diffusional behaviour accurately at intermediate and long times but the α profile follows a curve intermediate between the limiting cases at short times, namely before the curves given by the limiting cases cross. This suggests that, as θ_c is decreased from $\pi/2$, a transition to near-disk-like behaviour occurs first for the flux at long times, followed by a later transition for short times. This complicates determin-

ing the diffusional behaviour from the global (non-local) α profile alone as it depends on which point of time in the transient is considered.

To better understand this phenomenon, we extract profiles for the local diffusion indicator, α_{local} , to assess local diffusional effects. Fig. 11 presents α_{local} profiles at various points along the surface of (A) a sphere truncated to $\theta_c = \pi/4$ and (B) a sphere truncated to $\theta_c = \pi/8$. Plots of the curves predicted by the isolated sphere, “modified sphere” and Shoup-Szabo equations are presented by black, purple, and red dashed lines respectively. The position on the electrode surface from which the profiles are derived is given as the θ -coordinate in the Figure legends.

As was observed for $\theta_c > \pi/2$, all α_{local} profiles in Fig. 11 follow the same curve at short times. For the truncated spheres this curve is given by the isolated sphere equation. This curve represents the profiles that would be expected if material were to exclusively diffuse along the vector normal to the electrode surface at all times. Each plot exhibits a deviation from this curve once material begins to arrive along a vector parallel to the electrode surface. The larger the θ from which the α_{local} profile is taken (and thus the closer to the electrode surface's

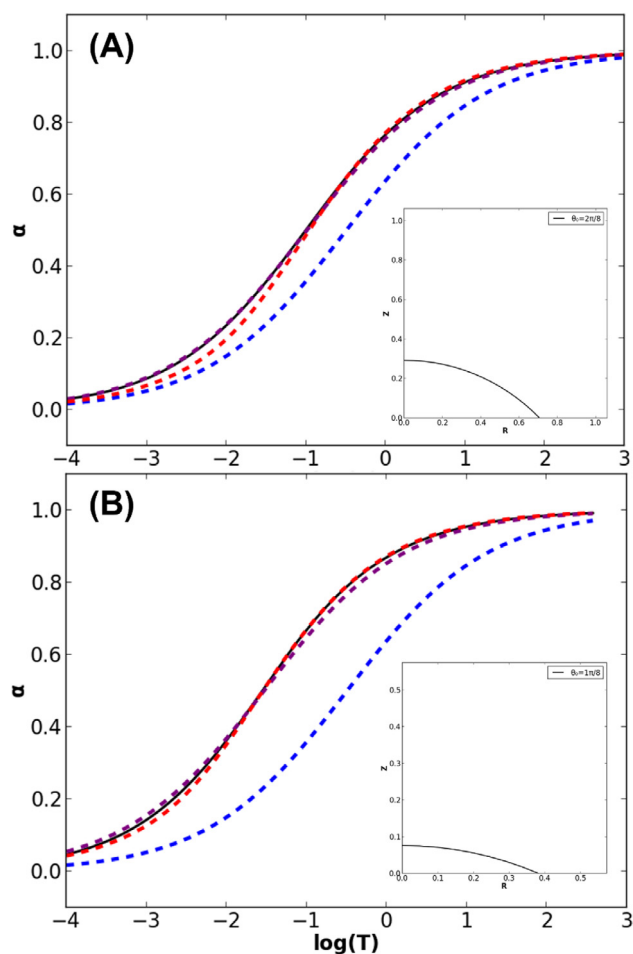


Fig. 10. Diffusion indicator (α) profiles for the truncated spheres with contact angles of (A) $\theta_c = \pi/4$ and (B) $\theta_c = \pi/8$ illustrated as black solid lines. Also presented are curves illustrating profiles for the isolated sphere (blue dashed), the “modified sphere” equation (purple dashed), and the Shoup-Szabo equation for a disk of equal surface area (red dashed). Inlaid diagrams illustrate the shapes of the corresponding truncated sphere electrodes on the supporting plane. Significant overlap between the solid black line and the purple dashed line in (A) and between the solid black line and the red dashed line in (B) makes distinguishing these curves difficult graphically at certain times.

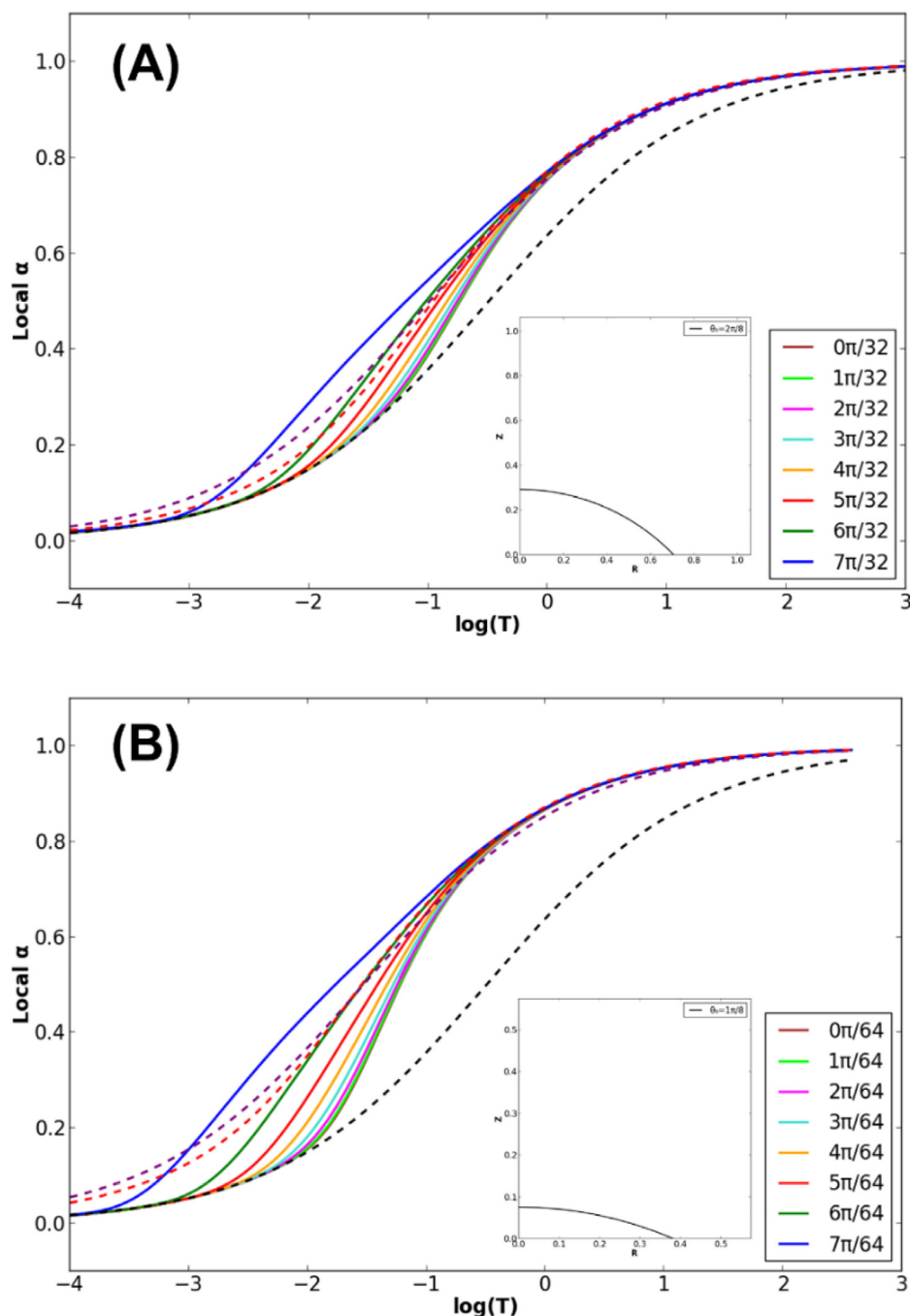


Fig. 11. Local diffusion indicator (α_{local}) profiles for the truncated spheres with contact angles of (A) $\theta_c = \pi/4$ and (B) $\theta_c = \pi/8$. Profiles for the isolated sphere (black dashed), the “modified sphere” equation (purple dashed), and the Shoup-Szabo equation for a disk of equal surface area (red dashed) are also presented. The position on the electrode surface from which a given α_{local} profile is extracted is given in the Figure legend as the θ -position. Inlaid diagrams illustrate the shape of the corresponding truncated sphere electrodes on the supporting plane.

edge), the earlier and the more pronounced the deviation. This is due to the greater influence of material arriving due to the edge effect.

The smaller the θ_c , the earlier this deviation occurs for all θ . This is further evidenced by comparison to the surface-local $\frac{\partial C}{\partial \theta}$ profiles given in Fig. 12 whereby positive $\frac{\partial C}{\partial \theta}$ maxima, produced by the arrival of material via the edge effect and followed by a decline towards steady state values, occur earlier and are more pronounced as θ_c decreases when comparing positions of equivalent θ/θ_c . As the contact angle decreases, it is seen that the response of the truncated sphere tends towards, but does not reach, the response of a flat disc, as shall be discussed below.

The long-time curve upon which the α_{local} profiles converge is equivalent to the long-time curve for the α profile. The convergence of α_{local} on to the α profile at long time is common to the geometries considered in this work. Since, at short times, α_{local} obeys the curve of normal diffusion, which depends only on the curvature of the electrode, it is emphasised that α_{local} 's principal utility is in the elucidation of diffusional effects intermediate between the diffusional regimes active at short and long times. As such, α_{local} is not useful for justifying the θ_c required for the truncated spheres to exhibit disk-like behaviour in the late time limit. However, comparison of the α_{local} profiles produced by simulation for the truncated spheres with the α_{local} profiles

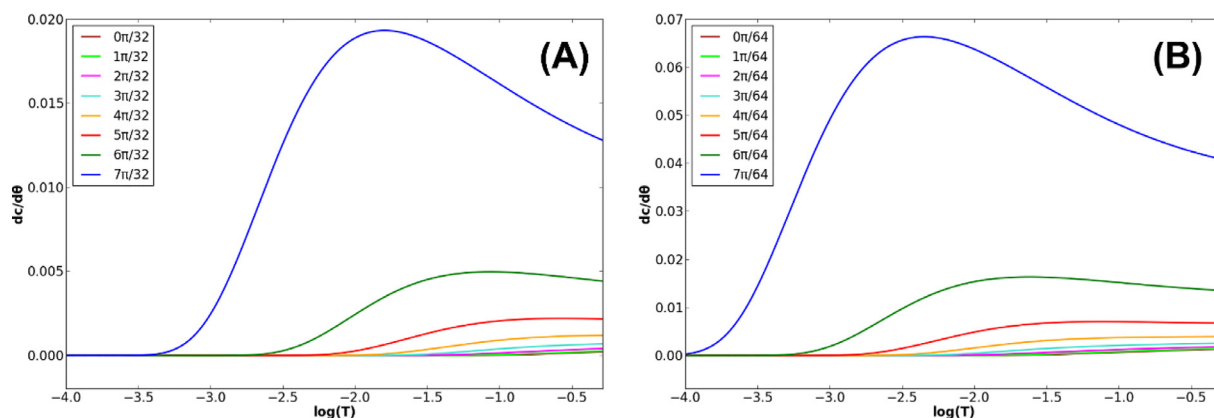


Fig. 12. Plots of local $\partial C/\partial \theta$ profiles on the electrode surface of truncated spheres with contact angles of (A) $\theta_c = \pi/4$ and (B) $\theta_c = \pi/8$. The θ -positions at which these profiles have been extracted have been given in the Figure legend.

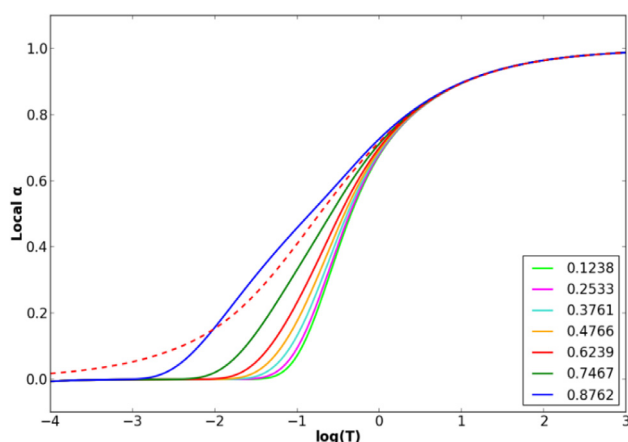


Fig. 13. Local diffusion indicator (α_{local}) profiles for a micro-disk electrode where variables are normalised to the disk radius as opposed to the radius of a spherical particle. The Shoup-Szabo equation is presented as the red dashed line. The R -position on the electrode surface from which a given α_{local} profile is extracted is given in the Figure legend.

produced by simulation for a microdisk yields valuable information about the linear-convergent diffusion regime transition.

Fig. 13 presents α_{local} profiles for a micro-disk extracted from various R -positions on the electrode surface, where R is the dimensionless

perpendicular distance from the axis of symmetry relative to the disk's radius. The profiles at early time all follow the response expected for Cottrellian diffusion of $\alpha = 0$. A deviation from this regime is seen once material begins to arrive along the dimension parallel to the electrode, which is the R -coordinate in the case of a microdisk. The α_{local} profiles converge at long times on to the long-time curve of the α profile which is accurately predicted by the Shoup-Szabo equation.

Correspondence of α_{local} for a truncated sphere to that observed for a microdisk is obscured by the influence of the isolated sphere equation, which deviates from Cottrellian diffusion at very early times. For truly disk-like behaviour to be observed across the entire transient for a truncated sphere, the edge effect must contribute greatly to the surface flux before diffusion to the curved surface can deviate from linearity. Thus near-disk-like behaviour is harder to achieve at short times for a truncated sphere compared to at long times.

Plots of $\frac{\partial \alpha_{local}}{\partial \log(T)}$ are presented in Fig. 14 to further investigate the shape of the α_{local} curves for truncated spheres of $\theta_c = \pi/4$ (A), $\theta_c = \pi/8$ (B), and for a microdisk (C). Curves corresponding to the isolated sphere (black dashed), the “modified sphere” (purple dashed), the Shoup-Szabo equation (red dashed) and purely linear diffusion (orange dashed) are co-presented for comparison. Note that in Fig. 14(C), the time domain is normalised to the disk radius and not a sphere radius, since the radius of a disk comparable to a given truncated sphere is dependent on θ_c .

It can be seen in Fig. 14 that two peaks are present in the gradients of α_{local} . The closer to the electrode edge, the greater the peak separation; however, for most of the electrode surface, the peaks are co-

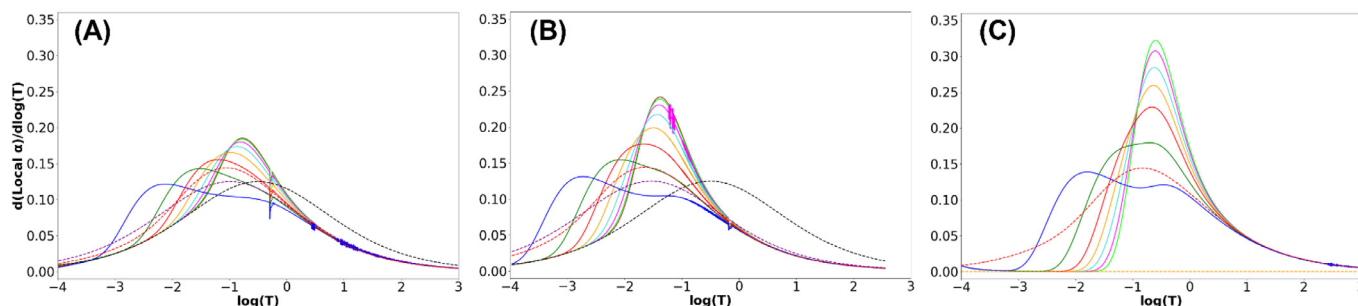


Fig. 14. Smoothed gradients of simulated α_{local} profiles ($d\alpha_{local}/d\log(T)$) for (A) $\theta_c = \pi/4$, (B) $\theta_c = \pi/8$, and (C) a microdisk. These curves are coloured according to the position on the active surface from which they were extracted in terms of θ/θ_c for (A) and (B) and in terms of R for (C). The colour scheme is as follows with the dimensionless positions given in brackets: dark blue (7/8), green (6/8), red (5/8), orange (4/8), light blue (3/8), purple (2/8), lime (1/8), and brown (at the symmetry axis). The time domain is normalised to the radius of the sphere for subplots (A) and (B) and to the radius of the microdisk for subplot (C). Curves corresponding to the isolated sphere (black dashed), the “modified sphere” (purple dashed), the Shoup-Szabo equation (red dashed) and purely linear diffusion (orange dashed) are co-presented for comparison.

lesced and indistinguishable. At long times, each profile converges together. The smaller the θ_c , the earlier the convergence. The curve upon which the profiles converge is dependent on the extent of disk-like behaviour at long times and thus intermediate between the predictions of the “modified sphere” and Shoup-Szabo equations for the truncated spheres, as discussed previously, while the microdisk converges on to the Shoup-Szabo equation.

The two overlapping peaks are caused by and thus characterise two distinct diffusional processes. The first process corresponds to the edge effect whereby material arrives along the vector parallel to the electrode surface from the volume beyond the electrode edge. The second process relates to the transition to general convergent diffusion as the diffusion layer thickness exceeds the electrode dimensions and is independent of diffusion parallel to the electrode surface.

Decreasing θ_c increases the height of each maximum and shifts each maximum to earlier T , with the microdisk (C) acting as the limiting case. This is caused by decreasing the absolute distance that material diffusing parallel to the surface needs to travel to access a point on the surface. The smaller the θ/θ_c , the greater the sensitivity of the height and position to changes in θ_c .

The features apparent in the $\partial\alpha_{local}/\partial\log(T)$ profiles characterise the processes governing how the diffusional behaviour varies with time and thus provides insightful visualisation of individual local diffusional processes.

4. Conclusions

Complex diffusional effects occur during the transition from overall linear to overall convergent diffusion regimes in the current–time transients for a (truncated)-sphere-on-a-plane electrode geometries, including a temporary, intermediary, thin-layer-like behaviour for spheres with $\theta_c > \pi/2$ and a θ_c -dependent edge effect for spheres with $\theta_c < \pi/2$. In the limit of a nearly flat electrode, the response tends to that of a disc electrode. Using α_{local} we can observe the effects which cause deviations from simple diffusional behaviour, including the source of error for the “modified sphere” equation. The observation is made that electrodes exhibiting long-time convergent diffusion demonstrate α_{local} profiles which converge under the long-time limit irrespective of position on the surface. α_{local} allows a means to sensitively characterise how the diffusional behaviour affects the local flux and provides effective insight into the effect of concentration gradients parallel to the electrode surface on the normal surface flux. The gradient of α_{local} profiles can distinguish between the action of different diffusional processes which are otherwise indistinguishable. This analytical tool is hence valuable for the understanding of flux transients produced by complex electrode geometries and the visualisation of their diffusional behaviour.

CRedit authorship contribution statement

Joseph R. Elliott: Methodology, Software, Validation, Formal analysis, Investigation, Writing – original draft, Visualization. **Richard G. Compton:** Conceptualization, Resources, Writing – review & editing, Supervision, Project administration.

Declaration of Competing Interest

The authors declare that they have no known competing financial interests or personal relationships that could have appeared to influence the work reported in this paper.

Acknowledgements

This work was supported by Syngenta and EPSRC via the EPSRC Industrial CASE award EP/V519741/1. The funders did not contribute

to this work aside financial support. The authors would like to thank Dr. Christopher Batchelor-McAuley for his assistance with implementing fully implicit methods for our numerical simulation.

References

- [1] S.R. Belding, F.W. Campbell, E.J.F. Dickinson, R.G. Compton, Nanoparticle-modified electrodes, *PCCP* 12 (37) (2010) 11208–11221.
- [2] B.J. Sanghavi, S.M. Mobin, P. Mathur, G.K. Lahiri, A.K. Srivastava, Biomimetic sensor for certain catecholamines employing copper(II) complex and silver nanoparticle modified glassy carbon paste electrode, *Biosens. Bioelectron.* 39 (1) (2013) 124–132.
- [3] N. Ben Messaoud, M.E. Ghica, C. Dridi, M. Ben Ali, C.M.A. Brett, Electrochemical sensor based on multiwalled carbon nanotube and gold nanoparticle modified electrode for the sensitive detection of bisphenol A, *Sens. Actuators, B* 253 (2017) 513–522.
- [4] Y. Tang, W. Cheng, Nanoparticle-Modified Electrode with Size- and Shape-Dependent Electrocatalytic Activities, *Langmuir* 29 (9) (2013) 3125–3132.
- [5] R. Miao, M. Yang, R.G. Compton, The electro-oxidation of hydrazine with palladium nanoparticle modified electrodes: dissecting chemical and physical effects: catalysis, surface roughness, or porosity?, *J. Phys. Chem. Lett.* 12 (28) (2021) 6661–6666.
- [6] Y.-Y. Bai, Z. Wu, C.-M. Xu, L. Zhang, J. Feng, D.-W. Pang, Z.-L. Zhang, One-to-Many Single Entity Electrochemistry Biosensing for Ultrasensitive Detection of microRNA, *Anal. Chem.* 92 (1) (2020) 853–858.
- [7] H. Ren, M.A. Edwards, Stochasticity in single-entity electrochemistry, *Curr. Opin. Electrochem.* 25 (2021) 100632, <https://doi.org/10.1016/j.coelec.2020.08.014>.
- [8] Y. Wang, X. Shan, N. Tao, Emerging tools for studying single entity electrochemistry, *Faraday Discuss.* 193 (2016) 9–39.
- [9] S. Eloul, E. Kätelhön, C. Batchelor-McAuley, K. Tschulik, R.G. Compton, Diffusional impacts of nanoparticles on microdisc and microwire electrodes: The limit of detection and first passage statistics, *J. Electroanal. Chem.* 755 (2015) 136–142.
- [10] W. Cheng, R.G. Compton, Electrochemical detection of nanoparticles by ‘nano-impact’ methods, *TrAC, Trends Anal. Chem.* 58 (2014) 79–89.
- [11] S.V. Sokolov, S. Eloul, E. Kätelhön, C. Batchelor-McAuley, R.G. Compton, Electrode–particle impacts: a users guide, *PCCP* 19 (1) (2017) 28–43.
- [12] X. Chang, C. Batchelor-McAuley, R.G. Compton, Methanol oxidation at single platinum nanoparticles, *J. Electroanal. Chem.* 896 (2021) 115438.
- [13] R.-C. Xie, C. Batchelor-McAuley, M. Yang, R.G. Compton, Substrate mediated dissolution of redox active nanoparticles; electron transfer over long distances, *Nano Res.* 15 (1) (2022) 429–437.
- [14] R.D. DeMars, I. Shain, Anodic Stripping Voltammetry Using the Hanging Mercury Drop Electrode, *Anal. Chem.* 29 (12) (1957) 1825–1827.
- [15] I. Streeter, R.G. Compton, Diffusion-limited currents to nanoparticles of various shapes supported on an electrode: spheres, hemispheres, and distorted spheres and hemispheres, *J. Phys. Chem. C* 111 (49) (2007) 18049–18054.
- [16] S.R. Belding, R.G. Compton, Transient voltammetry at electrodes modified with a random array of spherical nanoparticles: theory, *J. Phys. Chem. C* 114 (18) (2010) 8309–8319.
- [17] K.R. Ward, N.S. Lawrence, R. Seth Hartshorne, R.G. Compton, Modelling the steady state voltammetry of a single spherical nanoparticle on a surface, *J. Electroanal. Chem.* 683 (2012) 37–42.
- [18] P.A. Bobbert, M.M. Wind, J. Vlieger, Diffusion to a slowly growing truncated sphere on a substrate, *Physica A* 141 (1) (1987) 58–72.
- [19] H. Le, E. Kätelhön, R.G. Compton, Characterising the nature of diffusion via a new indicator: Microcylinder and microring electrodes, *J. Electroanal. Chem.* 855 (2019) 113602, <https://doi.org/10.1016/j.jelechem.2019.113602>.
- [20] H. Le, R.G. Compton, Comparative chronoamperometry: Spheres, discs, cylinders and bands, *J. Electroanal. Chem.* 866 (2020) 114149, <https://doi.org/10.1016/j.jelechem.2020.114149>.
- [21] C. Batchelor-McAuley, R.G. Compton, Diffusion to a cube: A 3D implicit finite difference method, *J. Electroanal. Chem.* 877 (2020) 114607.
- [22] O. Orrick, M. Yang, C. Batchelor-McAuley, R.G. Compton, Characterising Fickian diffusion on the surface of a sphere, *J. Electroanal. Chem.* 900 (2021) 115738.
- [23] R. Usha Rani, L. Rajendran, Diffusion indicator for hemispheroidal and ring ultramicroelectrode geometries for E and EC' reactions, *Electrochem. Commun.* 128 (2021) 107071.
- [24] R.G. Compton, E. Laborda, K. Ward, *Understanding voltammetry*, Third ed., World Scientific (2018).
- [25] A.J. Bard, L.R. Faulkner, C.G. Zoski, J. Leddy, *Electrochemical methods : fundamentals and applications*, Second ed. 2001.
- [26] A. Einstein, Über die von der molekularkinetischen Theorie der Wärme geforderte Bewegung von in ruhenden Flüssigkeiten suspendierten Teilchen, *Ann. Phys.* 322 (8) (1905) 549–560.
- [27] M. von Smoluchowski, Zur kinetischen Theorie der Brownschen Molekularbewegung und der Suspensionen, *Ann. Phys.* 326 (14) (1906) 756–780.
- [28] D.J. Gavaghan, An exponentially expanding mesh ideally suited to the fast and efficient simulation of diffusion processes at microdisc electrodes. 1. Derivation of the mesh, *J. Electroanal. Chem.* 456 (1–2) (1998) 1–12.
- [29] M. Rudolph, Digital Simulations on unequally spaced grids. Part 1. Critical remarks on using the point method by discretisation on a transformed grid, *J. Electroanal. Chem.* 529 (2) (2002) 97–108.
- [30] R. Seiber, S. Stefani, Explicit finite difference method in simulating electrode processes, *Anal. Chem.* 53 (7) (1981) 1011–1016.

- [31] S.W. Feldberg, Optimization of explicit finite-difference simulation of electrochemical phenomena utilizing an exponentially expanded space grid: Refinement of the Joslin-Pletcher algorithm, *J. Electroanal. Chem. Interfacial Electrochem.* 127 (1) (1981) 1–10.
- [32] J.A. Alden, R.G. Compton, A general method for electrochemical simulations. 1. Formulation of the strategy for two-dimensional simulations, *J. Phys. Chem. B* 101 (44) (1997) 8941–8954.
- [33] R.G. Compton, E. Kätelhön, E. Laborda, K.R. Ward, *Understanding voltammetry: Simulation of electrode processes*, Second ed., World Scientific Europe 2020.
- [34] P. Laasonen, Über eine Methode zur Lösung der Wärmeleitungs-gleichung, *Acta Mathematica* 81(none) (1949) 309–317, 9.
- [35] R.D. Falgout, U.M. Yang, *hypr: A Library of High Performance Preconditioners*, Springer, Berlin Heidelberg, Berlin, Heidelberg, 2002, pp. 632–641.
- [36] R.D. Falgout, J.E. Jones, U.M. Yang, *The Design and Implementation of hypr, a Library of Parallel High Performance Preconditioners*, Springer, Berlin Heidelberg, Berlin, Heidelberg, 2006, pp. 267–294.
- [37] J. Crank, *The Mathematics of Diffusion*, Clarendon Press, 1979.
- [38] J.R. Delmastro, D.E. Smith, Methods for obtaining approximate solutions to the expanding-sphere boundary value problem in direct current polarography, *J. Phys. Chem.* 71 (7) (1967) 2138–2149.
- [39] M. Lovrić, M. Branica, Application of ASV for Trace Metal Speciation II. Digital Simulation of Neopolarogram Using Hanging-mercury-drop Electrode, *Croatica Chemica Acta* 53 (3) (1980) 477–483.
- [40] A.M. Bond, K.B. Oldham, Potentiostatic voltammetry at the static mercury drop and other spherical electrodes, *J. Electroanal. Chem. Interfacial Electrochem.* 158 (2) (1983) 193–215.
- [41] C. Liu, W. Cheng, Q. Zeng, X. Huang, L. Wang, Voltammetric and microscopical investigation of the properties and behaviors of individual mercury micro-droplets, *J. Electroanal. Chem.* 784 (2017) 145–152.
- [42] B. Haddou, N.V. Rees, R.G. Compton, Nanoparticle–electrode impacts: the oxidation of copper nanoparticles has slow kinetics, *PCCP* 14 (39) (2012) 13612–13617.
- [43] Z. Guo, S.J. Percival, B.o. Zhang, Chemically Resolved Transient Collision Events of Single Electrocatalytic Nanoparticles, *J. Am. Chem. Soc.* 136 (25) (2014) 8879–8882.
- [44] E.N. Saw, M. Kratz, K. Tschulik, Time-resolved impact electrochemistry for quantitative measurement of single-nanoparticle reaction kinetics, *Nano Res.* 10 (11) (2017) 3680–3689.
- [45] F.G. Cottrell, Der Reststrom bei galvanischer Polarisation, betrachtet als ein Diffusionsproblem, *Z. Phys. Chem.* 42U (1) (1903) 385–431.
- [46] K.B. Oldham, Edge effects in semiinfinite diffusion, *J. Electroanal. Chem. Interfacial Electrochem.* 122 (1981) 1–17.
- [47] M. Yang, C. Batchelor-McAuley, E. Kätelhön, R. Compton, A New Approach to Characterising the Porosity of Particle Modified Electrodes: Potential Step Chronoamperometry and the Diffusion Indicator, *Applied Materials Today* In press (2021).
- [48] D. Shoup, A. Szabo, Chronoamperometric current at finite disk electrodes, *J. Electroanal. Chem. Interfacial Electrochem.* 140 (2) (1982) 237–245.
- [49] K. Aoki, J. Osteryoung, Diffusion-controlled current at the stationary finite disk electrode: Theory, *J. Electroanal. Chem.* 122 (C) (1981) 19–35.
- [50] K.B. Oldham, C.G. Zoski, Comparison of voltammetric steady states at hemispherical and disc microelectrodes, *J. Electroanal. Chem. Interfacial Electrochem.* 256 (1) (1988) 11–19.
- [51] D.J. Gavaghan, J.S. Rollett, Correction of boundary singularities in numerical simulation of time-dependent diffusion processes at unshielded disc electrodes, *J. Electroanal. Chem. Interfacial Electrochem.* 295 (1–2) (1990) 1–14.
- [52] R. Ferrigno, P.F. Brevet, H.H. Girault, Finite element simulation of the chronoamperometric response of recessed and protruding microdisc electrodes, *Electrochim. Acta* 42 (12) (1997) 1895–1903.
- [53] K. Aoki, Several Derivations for $I = 4Fc^*Da$, *Rev. Polarography* 63 (1) (2017) 21–28.
- [54] P.J. Mahon, K.B. Oldham, The transient current at the disk electrode under diffusion control: a new determination by the Cope-Tallman method, *Electrochim. Acta* 49 (28) (2004) 5041–5048.
- [55] P.J. Mahon, K.B. Oldham, Diffusion-Controlled Chronoamperometry at a Disk Electrode, *Anal. Chem.* 77 (18) (2005) 6100–6101.
- [56] L.K. Bieniasz, Highly accurate, inexpensive procedures for computing chronoamperometric current, integral transformation kernel, and related integrals, for an inlaid disk electrode, *Electrochim. Acta* 259 (2018) 1068–1080.